Anal Bioanal Chem (2009) 393:1835–1842
DOI 10.1007/s00216-008-2596-5

REVIEW

Three-dimensional depth profiling of molecular structures

A. Wucher · J. Cheng · L. Zheng · N. Winograd

Received: 5 September 2008 / Revised: 10 December 2008 / Accepted: 16 December 2008 / Published online: 20 January 2009
© Springer-Verlag 2009

Abstract Molecular time of flight secondary ion mass spectrometry (ToF-SIMS) imaging and cluster ion beam erosion are combined to perform a three-dimensional chemical analysis of molecular films. The resulting dataset allows a number of artifacts inherent in sputter depth profiling to be assessed. These artifacts arise from lateral inhomogeneities of either the erosion rate or the sample itself. Using a test structure based on a trehalose film deposited on Si, we demonstrate that the "local" depth resolution may approach values which are close to the physical limit introduced by the information depth of the (static) ToF-SIMS method itself.

Electronic supplementary material The online version of this article (doi:10.1007/s00216-008-2596-5) contains supplementary material, which is available to authorized users.

A. Wucher (✉)
Fachbereich Physik, Universität Duisburg-Essen,
47048 Duisburg, Germany
e-mail: andreas.wucher@uni-due.de

J. Cheng · L. Zheng · N. Winograd
Department of Chemistry, Pennsylvania State University,
104 Chemistry Bldg.,
University Park, PA 16802, USA

Present address:
J. Cheng
Merck & Co., Inc.,
WP78-210, 770 Sumneytown Pike,
West Point, PA 19486, USA

Present address:
L. Zheng
Evans Analytical Group,
810 Kifer Rd.,
Sunnyvale, CA 94086, USA

Keywords Biological samples · Electron/ion microprobe · Mass spectrometry/ICP-MS · Thin films

Introduction

The three-dimensional chemical characterization of thin-film structures requires analytical techniques which allow both lateral (i.e., parallel to the surface) and vertical (i.e., perpendicular to the surface) resolution on the nanometer scale. A prominent strategy for such investigations is to combine laterally resolved surface analysis with layer-by-layer sample erosion, thus gradually exposing the entire three-dimensional sample to the surface-sensitive analysis method. Among the various possible approaches, sputter depth profiling has evolved as one of the most versatile tools to obtain chemical information as a function of depth below the initial surface. In this technique, the solid is eroded by an energetic ion beam, which removes surface material due to sputtering. Combined with a mass spectrometric technique such as secondary ion mass spectrometry (SIMS) or secondary neutral mass spectrometry (SNMS) to characterize the sputtered material, this allows for a high-resolution three-dimensional analysis with lateral dimensions down to about 10 nm and depth resolution down to the nanometer range.

A particular strength of mass spectrometry is the analysis of molecular surfaces. It has long been demonstrated that the flux of material removed from such a surface under ion bombardment contains molecular species which are representative of the surface chemistry [1]. However, it was common knowledge that such an analysis had to be performed under "static" conditions, where the primary ion fluence was kept low enough to ensure that no point at the surface was influenced by more than one ion impact. If this condition was violated, chemical damage induced by

the ion impact accumulated, leading to a fast exponential decay of molecule-specific information with increasing ion fluence. It is clear that this precludes sputter depth profiling of molecular films, which was long deemed virtually impossible due to the damage accumulation effect.

Only recently, it was discovered that damage accumulation could be prevented if *cluster* projectiles instead of atomic ions were used to bombard the surface [2]. Not only were these projectiles found to greatly increase the yield of molecular species in the sputtered flux (thereby greatly enhancing their detection sensitivity, see [3, 4] for a review) but also to largely suppress the fluence-dependent disappearance of the molecular signal, thus opening the door for molecular sputter depth profiling applications. Consequently, a number of studies have been published where this molecular sputter depth profiling appears to work fairly well [2, 5–26], and insights into the underlying fundamental concepts are beginning to emerge.

Imaging mass spectrometry can be achieved in two different ways. In *microscope* mode, the surface is irradiated with an extended primary ion beam and a stigmatic 2D image of the emitted secondary ions is recorded with micrometer lateral resolution. In *microprobe* mode, on the other hand, the primary ion beam is finely focused and rastered across the surface, while all secondary ions emitted from the momentarily irradiated spot are analyzed. The recent advent of highly focusable cluster ion sources has brought about the possibility of molecular imaging with submicrometer lateral resolution. Combined with sputter depth profiling and a suitable method to obtain surface topography information, three-dimensional chemical analysis with molecular specificity has become feasible. In the present paper, we briefly describe such an analysis with particular emphasis on depth scale issues related to the conversion of the acquired data into quantitative 3D volumetric information.

Three-dimensional profiling

This section briefly reviews the standard protocol for 3D depth profiling along with a quantitative extension that has been developed recently in our laboratory [27, 28]. The experimental data reported below have been accumulated using standard time of flight (ToF)-SIMS instrumentation in combination with a fullerene cluster ion gun delivering C_{60}^{q+} ions of selectable charge state q=1...3 with kinetic energies up to several 10q keV. In some cases, mass spectral image acquisition is performed using the same focused fullerene ion beam as used for sputter erosion. Alternatively, the fullerene gun is solely used for sputter erosion, and the acquisition of SIMS images is performed using a liquid metal Au_n^+ or Bi_n^+ ion source. In order to obtain a chemical image of the momentary surface, the pulsed projectile ion beam is digitally rastered across an array of typically 256×256 pixels within a predefined field of view, and secondary ions sputtered from the currently bombarded spot are analyzed in the ToF spectrometer. All detected ions are recorded along with information regarding their flight time and the pixel from which they were acquired, thus allowing construction of mass selective ion images or area selective mass spectra after completion of the analysis.

Information about the vertical dimension along the surface normal (in the following referred to as “depth” or “height”) is obtained by acquiring a series of sequential images separated by sputtering cycles, where the surface is eroded by the ion beam. During these cycles, the fullerene projectile beam is operated in a dc mode and digitally rastered across the same field of view as used during data acquisition. This feature is important to note, since it is different from conventional sputter depth profiling applications (where data acquisition is restricted to a small portion of the erosion area in order to avoid crater effects). Typical dimensions of the raster field of view are $\Delta x \cdot \Delta y$ with Δx=200 µm, $\Delta y = \Delta x/\cos\theta$, and θ being the impact angle of the primary ion beam (typically around 45° with respect to the surface normal).

As part of a strategy for quantitative 3D profiling developed recently in our laboratory, the topography of the investigated surface is examined using a wide-area atomic force microscope (AFM). In order to determine the total depth eroded during the entire 3D analysis, AFM images are obtained both *prior to* and *after* the SIMS depth profile. Since the AFM data are taken outside the vacuum chamber, care must be taken regarding the time delay between AFM and SIMS data acquisition (typically about 30 min) to make sure that relaxation of the film after sputtering does not influence the results. Registration of the two AFM images is accomplished using surface markers, which must be located outside the area analyzed by the depth profile and therefore visible in both images. Since the height zero of AFM images is arbitrary, it was calibrated by matching the average height measured outside the depth profiled area in both images. Registration of the AFM images with the area analyzed in the SIMS depth profile is accomplished using the eroded sputter crater, which is clearly visible in the image obtained after the analysis. The resulting overlay is critical and must be closely examined using features that can (ideally) be identified in both the AFM and the SIMS images. By matching the pixel resolution of the AFM data with that of the SIMS images, pixel-resolved topography information before and after the depth profile analysis is generated, and the total depth eroded at each pixel of the analyzed area can be determined separately. This information is extremely important since the results reported below show that the erosion rate, i.e., the depth interval eroded per unit of projectile ion fluence,

may substantially vary between different positions within the analyzed area [27].

In order to arrive at true 3D information, the height coordinate of each voxel (i, j, k) corresponding to pixel (j, k) in image number (i) is calculated individually. In doing so, the local erosion rate is allowed to vary as a function of depth, for instance between different vertical layers of the sample structure. The chemical information obtained from the SIMS spectrum is used to interpolate the erosion rate for each voxel (i, j, k) individually, and calibration is achieved by integrating the erosion rate at a pixel position (j, k) over all erosion steps (i) and equating the result with the total eroded depth determined from the AFM measurement. Details of this nonlinear conversion have been described elsewhere [27, 28] and will not be repeated here. As a result, each secondary ion detected in the course of the entire depth profile analysis is tagged with an individual coordinate vector (x, y, z, t) describing its spatial origin (x, y, z) within the investigated sample volume along with its flight time t.

The resulting dataset can be analyzed in many different ways. First, a laterally gated depth profile of a particular species can be generated by binning all detected ions within the respective flight time interval (corresponding to a selected secondary ion mass) and subset of pixels (corresponding to the selected gating area) according to the depth coordinate z. The result is what is normally acquired in a conventional sputter depth profile, with, however, the big difference that the data are binned according to *actual height* rather than projectile ion fluence. In other words, different pixels of the same SIMS image are counted at different height, a notion which is impossible in conventional depth profiling. Variations of the erosion rate across the gated area, which inevitably distort a conventional profile, can therefore be assessed and corrected (see below).

Second, vertical images can be constructed in order to visualize cross sections of the analyzed sample volume. These images can be very useful to examine the sequence of vertical layers and, in particular, the interface between different layers. If, for any reason, the depth at which an interface is detected exhibits a lateral variation, then the interface width measured in a conventional depth profile will naturally be distorted. In a 3D profile, however, these effects can be visualized and corrected as described below.

Third, the data can be visualized in a graphical 3D representation, thus allowing us to identify the shape of different regions of interest within the analyzed sample volume. An example of such an analysis is shown in Fig. 1. The data were obtained from a 300-nm trehalose film deposited on Silicon and doped with a peptide at low concentration level (~1%). The film was prestructured using a 15-keV Ga^+ ion beam, leading to the erosion of a shallow crater of about 120×100 μm dimension and 30-nm depth. In addition, a few deep trenches were etched all the way through the overlayer to the underlying substrate, forming a pattern of the letters "PSU". In those areas where the sample had been exposed to the Ga^+ beam, gallium was implanted into the surface, which was later detected as a Ga^+ secondary ion signal in the ToF-SIMS spectra. The image shows isosurfaces of the resulting SIMS signals of the peptide dopant molecular ion (blue), the implanted gallium (red), and the silicon substrate (green). Animations of these surfaces viewed from different angles are available as Electronic Supplementary Material online. For better visibility, the isosurfaces were drawn with the signal downsampled over $5 \times 5 \times 5$ pixels, and intensity thresholds of 20 counts (Ga, Si) and one count (peptide) were used. The volume affected by the Ga^+ ion beam is clearly visible, revealing an implantation layer of about 50-nm thickness below the irradiated film surface. This volume is missing in the peptide image, revealing that the Ga^+ bombardment produced significant accumulation of chemical damage to the peptide molecules within the implantation layer. The same behavior is also found for the molecular ion signal of the trehalose matrix itself. Underneath the implantation layer, on the other hand, both the peptide and the trehalose molecular ions are being detected at the same intensity level as outside the surface regions affected by the Ga^+ beam. This finding is remarkable since it demonstrates that the $C_{60}{}^+$ cluster ion bombardment is capable to remove the sample volume damaged by the Ga^+ beam and uncover the unaffected molecular film below. For a detailed discussion of the data, the reader is referred to our previous publications [27, 28].

Depth resolution

One possible strategy to investigate the depth resolution is to determine the apparent width of interfaces between subsequent vertical layers. For the case of an organic film on an inorganic substrate, the depth resolution can be identified from the decrease of film-specific molecular signal and the simultaneous increase of substrate-related signal at the film–substrate interface. If the film thickness is large compared to the depth resolution of the analysis, the interface width Δz can be determined from the 16% to 84% transition of the respective secondary ion signals. If Δz becomes comparable to the film thickness, the analysis becomes more complicated. An example for this situation would be a multilayer stack of thin organic films, where the individual layer thickness is too small to allow the respective SIMS signal to reach a plateau during its removal. In this case, the depth resolution can be determined from the modulation contrast of the signals representing the different layers [18].

In any case, a proper assessment of Δz is not straightforward since the erosion rate may exhibit strong variations while profiling across an interface. This is

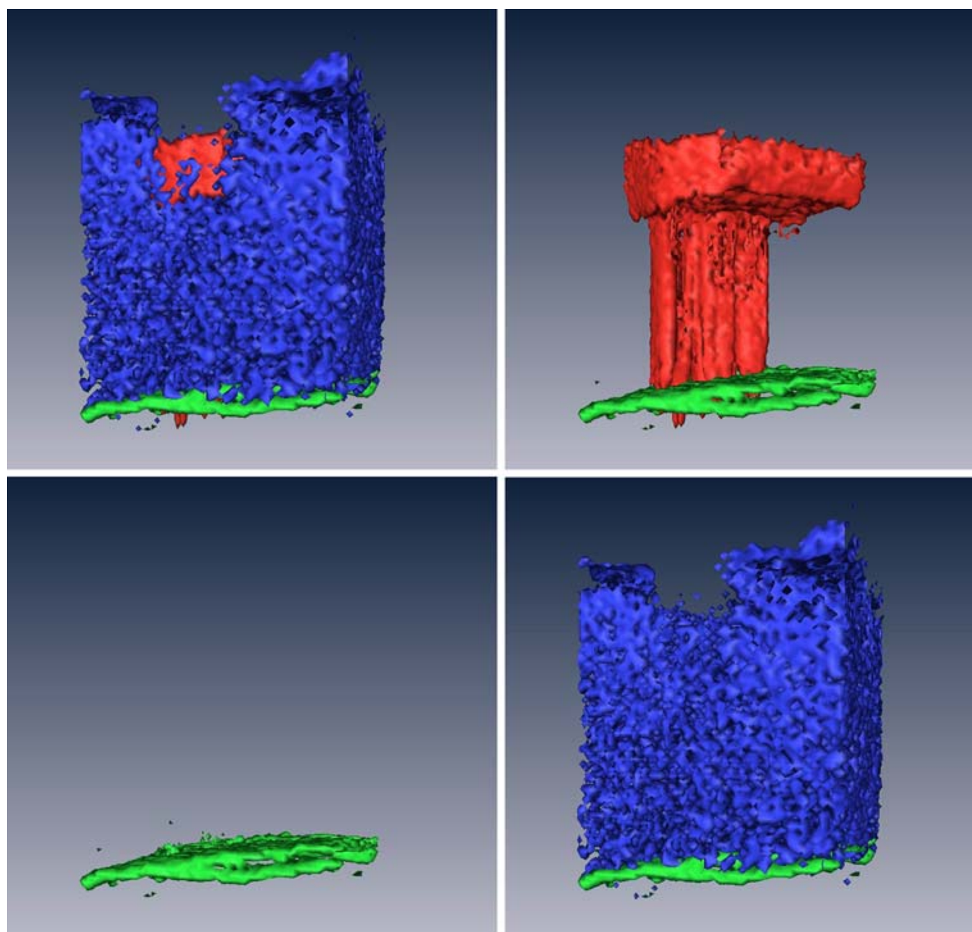

Fig. 1 Isosurface representation of a molecular 3D profile measured on a 300-nm trehalose film in Si which was prestructured using a Ga^+ ion beam. *Red*: Ga^+ secondary ion signal representing gallium-implanted material; *blue*: molecular ion signal representing a peptide doped into the trehalose film; *green*: Si^+ substrate signal (animations available online as Electronic Supplementary Material)

particularly important for a film–substrate interface, where the sputter yield and, hence, the erosion rate may vary by orders of magnitude between an organic film and the substrate material. In many cases, erosion practically stops once the substrate is reached, making the interface appear very broad in plots of signal intensity vs. projectile ion fluence. In principle, the same effect with, however, reduced magnitude will also generally occur for interfaces between different organic layers.

An accurate correction for the erosion rate variation across an interface is difficult. As a first-order approximation, one can interpolate the erosion rate between layers composed of material A and B as a function of ion fluence f according to

$$\frac{dz}{df} = c_A(f) \cdot \left.\frac{dz}{df}\right|_A + c_B(f) \cdot \left.\frac{dz}{df}\right|_B \qquad (1)$$

with weight factors $c_{A,B}$ calculated from the SIMS signals representing A and B, respectively. Different methods to calculate $c_{A,B}$ have been proposed [14, 15, 20, 29], all leading to qualitatively similar results with only subtle differences. Note, however, that there is not necessarily a sound physical basis for the validity of Eq. 1 since sputter yields of multicomponent systems may exhibit large nonlinearities as a function of chemical composition [30]. Note also that Eq. 1 leads to a nonlinear conversion of primary ion fluence into eroded depth, which in a three-dimensionally structured sample might be different for every voxel within the analyzed volume.

A number of factors may contribute to the measured interface width. These can be classified into three different categories, which are discussed below.

Lateral inhomogeneities

Lateral inhomogeneity effects can be caused by instrumental artifacts, the sample itself, or by the applied analysis method. A typical instrumental artifact is a lateral inhomogeneity of the projectile current density applied by the rastered ion beam during the erosion cycles. Such artifacts directly translate into a lateral variation of the erosion rate, leading to the development of macroscopic surface topography at the bottom of the eroded crater. It is obvious that this must act to broaden the observed interface since different crater depths are sampled at the same projectile ion fluence. Alternatively, the sample itself can exhibit a lateral variation of the molecular film thickness prior to depth profile analysis, which will then of course locate the interface at different ion

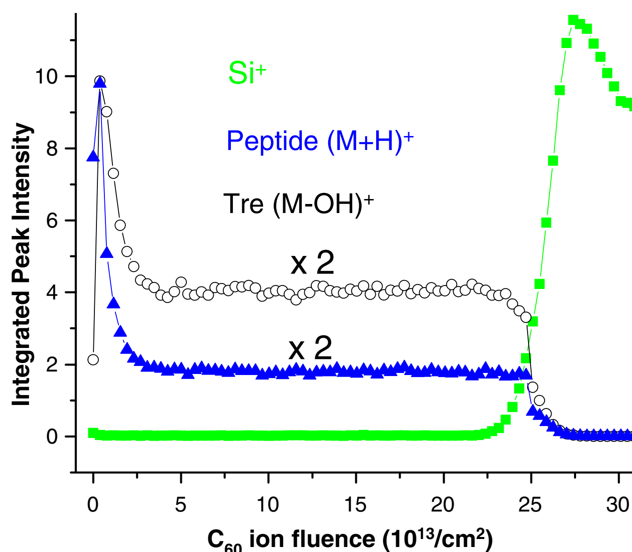

Fig. 2 Gated area depth profile of a 300-nm trehalose film doped with GGYR peptide on Si measured using 40-keV C_{60}^{+} projectile ions for sputter erosion and data acquisition. The gating area was 25% of the eroded crater area (280×200 μm)

fluence. Last but not least, the statistical nature of the sputtering process can lead to a fluence-dependent microscopic roughening of the surface, leading to short-scale fluctuations of the actually sampled depth.

Interface mixing

Mixing effects are well known in sputter depth profiling. The energy introduced into the solid due to the ion bombardment generates many displacements within a subsurface region, and molecules can be relocated across the original interface. This is a dynamical effect which is caused during the erosion cycles and cannot be avoided in a sputter depth profile. It can be expected to significantly influence the interface width observed between two different molecular films but should not be severe for a film–substrate interface since it is hard to imagine that intact molecules could be mixed into the very dense inorganic substrate lattice without being fragmented. In the latter case, on the other hand, they cannot contribute to the molecule-specific ion signal any longer and therefore cannot affect the decay profile of this signal at the interface.

Information depth

The information depth of the (static) analysis method employed to characterize the chemistry of the momentarily exposed surface represents the ultimate physical limit of the observable interface width. For the cluster-ion-beam-initiated ToF-SIMS experiments described here, this quantity is determined by the depth of origin of the sputtered material, which is limited by the depth of the crater formed during a single impact event. Molecular dynamics simulations indicate that this leads to an intrinsic depth resolution of 2...3 nm depending on impact energy and angle [31–33]. The data suggest that the depth resolution can be improved by increasing the impact angle to grazing incidence, a notion which is also supported by experimental data [21, 22, 34]. Note, however, that the simulations were performed at significantly lower impact energy (5 keV) than employed here. It is not clear how the results extrapolate to the conditions of the experiments presented below. Data obtained for a pure metallic sample indicate the crater depth to slowly increase with increasing impact energy [35], a finding which appears to be consistent with experimental data of measured interface widths [22, 24].

Data analysis

In the following, we demonstrate how 3D depth profiling can help to unravel some of the physics determining the apparent depth resolution in molecular sputter depth profiling. For that purpose, we revisit published results obtained on three-model systems, namely (1) an organic film (peptide-doped trehalose) on a silicon substrate [14, 15, 20, 24, 36, 37], (2) a multilayer stack of alternating Langmuir-Blodgett films (barium-arachidate (AA) and barium dimyristoyl phosphatidate (DMPA) on silicon [18, 22, 23], and (3) a sequence of Irganox 3114 delta layers in an Irganox 1010 matrix [26].

A gated area depth profile determined from a dataset similar to the one displayed in Fig. 1 is shown in Fig. 2. A very fast initial rise of both the trehalose and the peptide

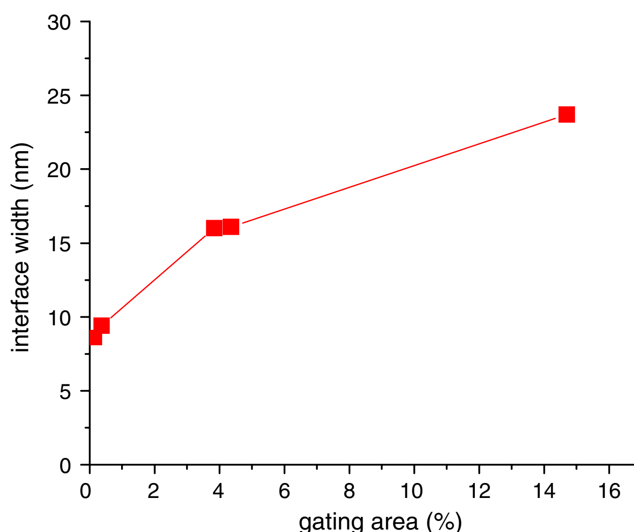

Fig. 3 Interface width determined for the film–substrate interface in Fig. 2 as a function of the gating area (given in percent of the eroded crater area). Lateral dimensions of the eroded crater 280×200 μm

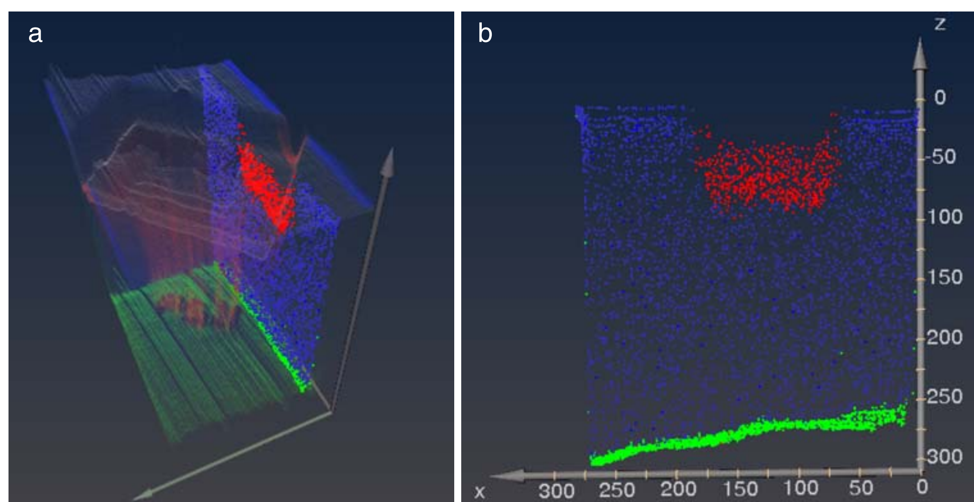

Fig. 4 **a**, **b** Vertical cross section image of the data depicted in Fig. 1. The signals representing the trehalose film (*blue*), the Si substrate (*green*), and the Ga implant (*red*) are plotted against the lateral coordinate *x* (in micrometer) and the depth below the original surface *z* (in nanometer)

molecular ion signal is followed by an exponential decay into a steady state, which then persists throughout the complete removal of the film. These features are typical for a molecular sputter depth profile and have been interpreted in terms of a simple erosion dynamics model describing the competition between ion-beam-induced damage and sputter removal of the intact molecules at the bombarded surface [15, 38]. The interface to the silicon substrate is clearly visible by the decay of the trehalose matrix and peptide dopant signals representing the film and the simultaneous rise of the silicon substrate signal. Using the erosion rate interpolation described above, an interface width of about 18 nm is determined, which slowly increases with increasing projectile impact energy to about 23 nm at 120 keV [24].

Note that the data in Fig. 2 were obtained by integrating the measured signal over a relatively large gating area with half the lateral dimensions of the sputter erosion crater. In order to examine whether the observed depth resolution is influenced by large-scale lateral inhomogeneity effects, one can reanalyze the 3D dataset and shrink the gating area to determine a smaller-field depth profile. As a result, the interface width is found to decrease with decreasing gating area as shown in Fig. 3. The smallest field of view from which it is possible to extract a meaningful depth profile contains about 100 pixels, corresponding to a lateral gating area of about $11\times 8\ \mu m^2$. Extrapolating the data in Fig. 3 to zero area, we find a "point" interface width of about 8 nm (at 40-keV impact energy), indicating that more than half of the originally observed width is caused by lateral inhomogeneity of either the sample or the erosion process.

To further discriminate between these two possibilities, we plot in Fig. 4b a vertical cross section image of the 3D data displayed in Fig. 1. The location of the cross section is shown in Fig. 4a. The image in Fig. 4b shows the signals representing the organic film (blue), the silicon substrate (green), and the gallium implant (red) plotted against the lateral coordinate (x) and the calibrated depth below the original surface (z). It is immediately evident that the interface is located at different depths depending on the lateral position within the analyzed surface area. Note that the depth axis is calibrated to reproduce the actually eroded total depth on each pixel (measured by AFM). Therefore, the seemingly curved shape of the silicon substrate surface clearly indicates a lateral variation of the trehalose film thickness, which amounts to about 40 nm across the entire analyzed area of about 280 μm. In reality, the silicon

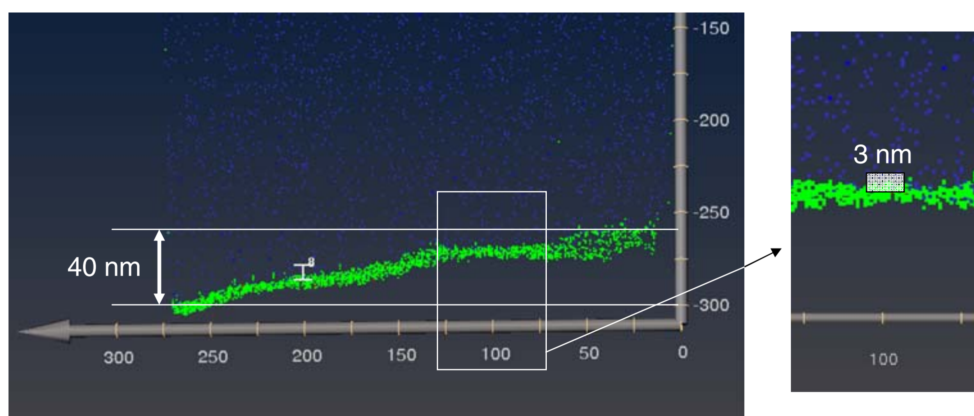

Fig. 5 Zoom of the vertical image displayed in Fig. 4b. *Horizontal axis*: lateral coordinate *x* (in micrometer); *vertical axis*: depth below the original surface *z* (in nanometer)

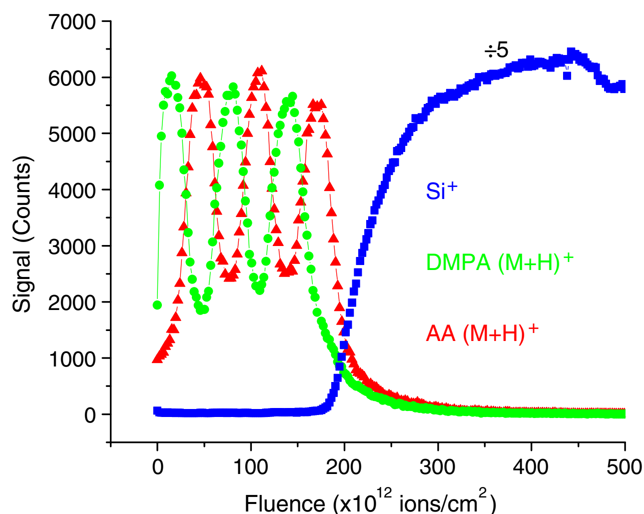

Fig. 6 Gated area depth profile of a multilayer stack of alternating LB films of about 50-nm width on Si measured using 40-keV C_{60}^+ projectile ions for sputter erosion and data acquisition. The gating area was 25% of the eroded crater area (280×200 μm)

substrate surface is of course flat, and the initial film surface is tilted, but such a gradual slope is automatically corrected by the AFM data acquisition software and, hence, not visible in the AFM data.

A close inspection of the interface region is shown in Fig. 5. From these data, it is immediately evident that an apparent interface broadening of about 10 nm *must* be measured if the gating area encloses the central 100 μm of the analyzed area. Our extrapolated zero-area width of 8 nm has been included as a vertical marker bar. It is evident that the actual interface width may even be smaller, as shown by the 3-nm bar depicted in the insert. From visual inspection of the data, we conclude that the actual interface width observed in this system must be close to the intrinsic limit of about 3 nm estimated from MD simulations.

As an example demonstrating film–film interface resolution, a gated area depth profile across an LB multilayer stack with about 50-nm individual layer thickness is shown in Fig. 6 [22]. It is seen that all six layers are clearly resolved. The fact that the signal does not reach a real plateau during removal of an individual layer indicates that the depth resolution must be of the order of about half the film thickness. This notion is corroborated by the analysis of the signal modulation contrast [18], which yields an apparent depth resolution of about 17 nm for the first interface between the top DMPA and the underlying AA layer. With a gating area analysis like that depicted in Fig. 3, the presence of lateral inhomogeneity artifacts are revealed in this case as well [39]. The corrected “interface width” (i.e., the full width at half maximum of the Gaussian depth response function extrapolated to zero gating area) is ~20% smaller than that obtained from Fig. 6.

Another observation is the degradation of depth resolution with increasing eroded depth as shown in Fig. 7a. Similar results have been found [26] for a sequence of Irganox 3114 delta layers embedded in an Irganox 1010 matrix analyzed by 30-keV C_{60}^+ ions (see Fig. 7b). As explained above, artifacts of this type can in principle arise from accumulated interface mixing as well as from bombardment-induced topography formation, the latter being either macroscopic (i.e., a crater effect induced by a lateral inhomogeneity of the sputter erosion rate) or microscopic (i.e., bombardment-induced roughening) in nature. While the observed linear dependence would be a natural consequence of a crater effect, this is not obvious for the development of bombardment-induced roughness. By AFM analysis of the erosion crater bottom at various eroded depths, the effect observed in Fig. 7b was entirely attributed to increasing surface roughness [26], while this influence was virtually excluded as a cause of the effect observed in Fig. 7a [22]. In the latter case, a careful analysis reveals that the observed degradation

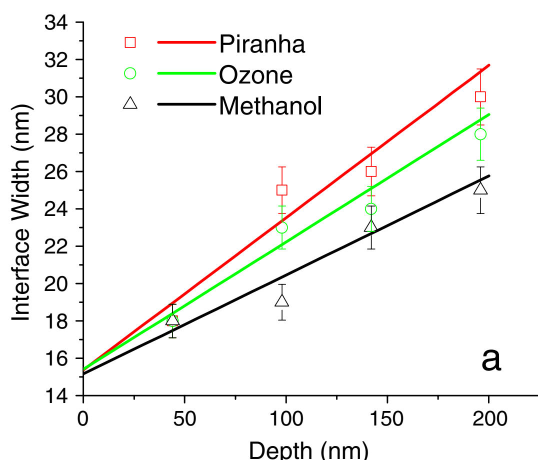

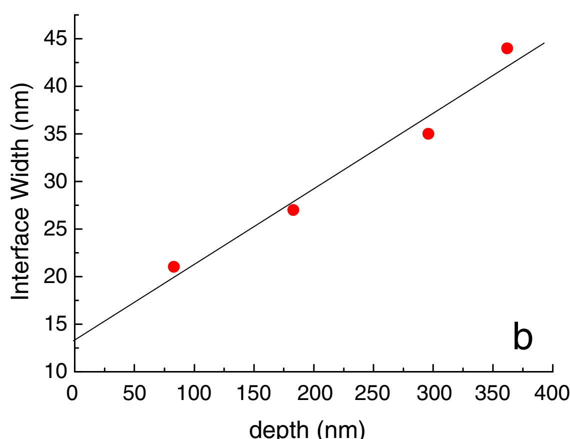

Fig. 7 Dependence of measured apparent depth resolution on total eroded depth as measured on **a** a multilayer stack of LB films [22] and **b** a sequence of Irganox 2019 delta layers in an Irganox 1010 matrix [26]

of depth resolution contains a small contribution from a macroscopic crater effect, but this cannot explain the effect alone. In this context, it is interesting to note that the slope observed in Fig. 7a was found to depend on the *original* roughness of the substrate *before* deposition of the LB multilayer, a finding which is still not completely understood.

Conclusions

The model systems reported here demonstrate that true 3D sputter depth profile analysis of molecular films appears feasible, provided the variation of the erosion rate both as a function of ion fluence and lateral position is taken into account. If, on the other hand, the erosion rate variation is neglected, a pseudo-3D representation of the measured image stack is obtained which in some cases may be strongly misleading.

The data presented here illustrate how 3D analysis can help to identify and possibly eliminate depth profiling artifacts that are caused by lateral inhomogeneities of either the erosion rate or—even more important—the sample itself. Compared to conventional depth profile analysis, the big advantage is that such effects can be directly assessed from the acquired dataset, and depth profiles obtained at different lateral positions and with different gating area can be compared without the need to repeat the analysis. As a consequence, the gating area can be retrospectively selected to optimize the inevitable compromise between detection sensitivity on one hand (requiring the gating area to be large) and depth resolution on the other hand (requiring the gating area to be small). In principle, one could imagine performing this optimization for different masses individually, so that the depth resolution could be optimized using a high-intensity matrix signal, while a low-intensity analyte signal (the peptide in our example) can be profiled with higher sensitivity.

Acknowledgements Financial support from the National Institute of Health under grant # EB002016-15, the National Science Foundation under grant # CHE-0555314, and the Department of Energy grant # DE-FG02-06ER15803 are acknowledged.

References

1. Benninghoven A, Rüdenauer FG, Werner HW (1987) Secondary ion mass spectrometry: basic concepts, instrumental aspects and trends. Wiley, New York
2. Gillen G, Lance K, Freibaum B, Lareau RT, Bennett J, Chmara F (2001) J Vac Sci Technol 19:568–575
3. Winograd N (2005) Anal Chem 77:142A–149A
4. Wucher A (2006) Appl Surf Sci 252:6482–6489
5. Gillen G, Roberson S (1998) Rapid Commun Mass Sp 12:1303–1312
6. Fuoco ER, Gillen G, Wijesundara MBJ, Muthu BJ, Wallace WE, Hanley L (2001) J Phys Chem B 105:3950–3956
7. Gillen G, Fahey A (2003) Appl Surf Sci 203–204:209–213
8. Weibel DE, Wong S, Lockyer N, Blenkinsopp P, Hill R, Vickerman JC (2003) Anal Chem 75:1754–1764
9. Wucher A, Sun S, Szakal C, Winograd N (2004) Appl Surf Sci 231–232:68–71
10. Mahoney C, Roberson S, Gillen G (2004) Anal Chem 76:3199–3207
11. Wagner MS, Gillen G (2004) Appl Surf Sci 231–232:169–173
12. Wagner MS (2005) Anal Chem 77:911–922
13. Mahoney C, Gillen G, Fahey A, Zu Ch, Batteas J (2005) Appl Surf Sci 252:6502–6505
14. Cheng J, Winograd N (2005) Anal Chem 77:3651–3659
15. Cheng J, Wucher A, Winograd N (2006) J Phys Chem B 110:8329–8336
16. Gillen G, Fahey A, Wagner M, Mahoney C (2006) Appl Surf Sci 252:6537–6541
17. Fletcher JS, Conlan XA, Lockyer N, Vickerman JC (2006) Appl Surf Sci 252:6513–6516
18. Zheng L, Wucher A, Winograd N (2007) J Am Soc Mass Spectrom 19:96–102
19. Mahoney C, Fahey A, Gillen G (2007) Anal Chem 79:828–836
20. Wucher A, Cheng J, Winograd N (2008) Appl Surf Sci 255:959–961
21. Kozole J, Wucher A, Winograd N (2008) Anal Chem 80:5293–5301
22. Zheng L, Wucher A, Winograd N (2008) Anal Chem 80:7363–7371
23. Zheng L, Wucher A, Winograd N (2008) Appl Surf Sci 255:816–818
24. Wucher A, Cheng J, Winograd N (2008) J Phys Chem C 112:16550–16555
25. Jones EA, Lockyer NP, Vickerman JC (2008) Anal Chem 80:2125–2132
26. Shard AG, Green FM, Brewer PJ, Seah MP, Gilmore IS (2008) J Phys Chem B 112:2596–2605
27. Wucher A, Cheng J, Winograd N (2007) Anal Chem 79:5529–5539
28. Wucher A, Cheng J, Zheng L, Willingham D, Winograd N (2008) Appl Surf Sci 255:984–986
29. Wagner MS (2004) Anal Chem 76:1264–1272
30. Betz G, Wehner GK (1983) Sputtering of multicomponent materials. In: Behrisch R (ed) Sputtering by particle bombardment, vol. 2. Springer, Heidelberg
31. Ryan KE, Smiley EJ, Winograd N, Garrison BJ (2008) Appl Surf Sci 255:844–846
32. Smiley EJ, Winograd N, Garrison BJ (2007) Anal Chem 79:494–499
33. Smiley EJ, Wojciechowski IA, Postawa Z, Winograd N, Garrison BJ (2006) Appl Surf Sci 252:6436–6439
34. Kozole J, Willingham D, Winograd N (2008) Appl Surf Sci 255:1068–1070
35. Postawa Z, Czerwinski B, Szewczyk M, Smiley EJ, Winograd N, Garrison BJ (2004) J Phys Chem B 108:7831–7838
36. Cheng J, Winograd N (2006) Appl Surf Sci 252:6498–6501
37. Cheng J, Kozole J, Hengstebeck R, Winograd N (2006) J Am Soc Mass Spectrom 18:406–412
38. Wucher A (2008) Surf Interface Anal 40:1545–1551
39. Zheng L, Wucher A, Winograd N (2009) in press